Tyrosine Kinase Inhibitors Diminish Renal Neoplasms in a Tuberous Sclerosis Model Via Induction of Apoptosis

Uchenna Unachukwu[1], Jarrod Sonett[1], Denzel Woode[1], Takayuki Shiomi[2], Kiran Chada[3], and Jeanine M. D'Armiento[1]

ABSTRACT

Tuberous sclerosis complex (TSC) tumors are presently incurable despite a cytostatic response to mTOR pathway inhibition because recurrence of disease occurs after treatment is discontinued. Here, we explored the hypothesis that inhibiting tyrosine kinase activity in mesenchymal lineage-specific platelet-derived growth factor receptor β (PDGFRβ) signaling in TSC tumors is cytocidal and attenuates tumorigenesis at significantly higher levels than treatment with an mTOR inhibitor. Rapamycin-induced versus tyrosine kinase inhibitor (TKI)–induced renal angiomyolipoma (AML) and pulmonary lymphangioleiomyomatosis (LAM) tumor cells were comparatively analyzed using cell survival assays, RNA sequencing, and bioinformatics to distinguish tumoricidal mechanisms adopted by each drug type. The efficacy of imatinib therapy was validated against spontaneously developing renal cystadenomas in tuberous sclerosis $Tsc2^{+/-}$ mouse models (C57BL/6J mice; $N = 6$; 400 mg/kg/d; oral gavage) compared with $Tsc2^{+/-}$ mice treated with PBS (C57BL/6J mice; $N = 6$). Our study revealed that TKIs imatinib and nilotinib were cytocidal to both pulmonary LAM and renal AML cell cultures through the downregulation of the glycoprotein GPVI pathway and resultant disruption in mitochondrial permeability, increased cytosolic cytochrome C, and caspase 3 activation. Importantly, renal tumor growth was significantly attenuated in imatinib-treated $Tsc2^{+/-}$ mice compared with PBS treatment. The preclinical studies reported here provide evidence documenting the effectiveness of TKIs in limiting LAM and AML cell growth and viability with important clinical potential. Furthermore, these drugs elicit their effects by targeting a PDGF pathway-dependent apoptotic mechanism supporting the investigation of these drugs as a novel class of TSC therapeutics.

Introduction

Tuberous sclerosis (TSC) has been attributed to loss-of-function mutations in either *TSC1* or *TSC2* tumor suppressor genes (1) leading to aberrant activation of the mTOR complex (mTORC1/2), dysfunctional cell proliferation, and neoplastic growth in multiple organs (2). Evidence of mTOR pathway inactivation in many studies of TSC tumors (3) also suggests that biochemical signaling due to activation of the mTOR pathway might not wholly account for the pathogenic phenotypes observed in TSC. The ELT-245 cell line was recently generated from uterine leiomyoma of the Eker rat model of TSC, which were therapeutically unresponsive to mTOR pathway inhibitors (4), as were some Eker rat renal tumors (5). In addition, many downstream effects of *TSC1/2* mutations have been shown to be tumorigenic independent of mTOR pathway activation (6, 7). Patients with TSC develop renal angiomyolipomas (AML; ref. 8) and other abnormalities in multiple organs (9). The pulmonary manifestation of TSC, lymphangioleiomyomatosis (TSC–LAM) occur almost exclusively in postpubertal women, causing cystic lung destruction, chylous pleural effusions, and pneumothorax (10). Because FDA-approved mTOR inhibitors such as rapamycin exert mainly tumoristatic effects at physiologic doses (11), a cytocidal therapeutic strategy that limits tumor growth and poor clinical outcomes is urgently needed.

TSC and LAM lesions present with heterogeneous mesenchymal cellular phenotypes (8), which can actively proliferate through the platelet-derived growth factor (PDGF) pathway signaling (12). This pathway transduces both tumorigenic and nontumorigenic signals via its transmembrane receptor tyrosine kinase to activate either the PI3K/Akt/mTOR pathway or the MAPK cascade (13). Activated PDGFRs recruit PI3K, which converts phosphatidylinositol-4,5-biphosphate (PIP2) into phosphatydlinositol-3,4,5-triphosphate (PIP3) that phosphorylates Akt. Phospho-Akt in turn inactivates TSC2 ultimately resulting in mTOR activation (14). PDGF signaling could thus account for the varied biological transformations causing TSC disorders, and both increases and decreases in PDGFR expression have been observed in cells with mono- or bi-allelic *Tsc2* mutations in several studies (14, 15). As such, pharmacologic perturbation of PDGF signaling posits an intriguing alternative or adjunctive to mTOR-based therapy for TSC and LAM tumorigenesis (16).

Therefore, in this study, we explored the effect of receptor tyrosine kinase inhibitors (TKIs), imatinib and nilotinib, on growth and viability of renal angiomyolipoma (AML) cells and dissociated cells from a lung tumor biopsy of a patient diagnosed with LAM. Imatinib is known for inhibiting the BCR-Abl1 and c-Kit tyrosine kinases as FDA-approved treatment of chronic myeloid leukemia (CML; ref. 17) and gastrointestinal stromal tumors (GIST; ref. 18), respectively. Imatinib exhibits an antiproliferative effect on mesenchymal cells through inhibition of phosphorylation/activation of both PDGFRα and PDGFRβ and is effective in the treatment of multiple cancers (19). Second-generation TKI nilotinib is also effective against imatinib-resistant CML and inhibits PDGFRs to modulate mesenchymal

[1]Department of Anesthesiology, College of Physicians and Surgeons, Center for LAM and Rare Lung Disease, Columbia University, New York, New York. [2]Department of Pathology, International University of Health and Welfare, School of Medicine, Chiba, Japan. [3]Department of Biochemistry, Rutgers-Robert Wood Johnson Medical School, Rutgers University, Piscataway, New Jersey.

Corresponding Author: Jeanine M. D'Armiento, Anesthesiology, ColumbiaUniversity College of Physicians & Surgeons, 630 West 168th Street, P&S 7-421, New York, NY 10032. E-mail: jmd12@cumc.columbia.edu

Mol Cancer Ther 2023;22:844–58

doi: 10.1158/1535-7163.MCT-22-0224

tumorigenesis and tissue differentiation processes (20). Given the mesenchymal ontology of TSC and LAM, we hypothesized that imatinib mesylate could exhibit tumoricidal properties superior to the tumoristatic effects of mTOR inhibitors. Using both cell-based assays and animal studies, we demonstrate that imatinib inhibits tumor growth and mechanistically deactivates the GPVI pathway inducing mitochondrial membrane permeability leading to caspase 3 activation and tumor cell death by apoptosis.

Materials and Methods

Cell lines and culture

Primary human renal angiomyolipoma (renal AML) cells immortalized with hTERT and SV40 T antigen (RRID:CVCL_C471, No. UMB1949 ATCC CRL4004; male; ref. 21) containing a defined 5bp deletion in exon 33 of *TSC2* leading to a frameshift mutation [p.Q1440fs; dbSNP ID:rs4517337; single-nucleotide polymorphism (SNP%) = 33%], a missense nonsynonymous bi-allelic G>A mutation at *TSC2* exon 16 causing pathogenic p.R611Q amino acid change [dbSNP ID: rs28934872; minor allele frequency (MAF): A = 0.002 (ALFA); SNP% = 100%] were obtained from ATCC. The SNP% is the percentage of sequence at a position in the assembly, which varies from the reference sequence. Primary human renal proximal tubule epithelial cells (RPTEC; No. PCS-400–010) and primary human lung fibroblasts (NLF; No. PCS-201–013) were obtained from ATCC. Primary human airway smooth muscle cells (HASMCs) were a kind gift from Dr. Monica Goldklang (Columbia University Medical Center) and have been characterized previously (22). Renal AML cells were maintained in culture using DMEM (No. 30–2002; ATCC) containing 10% FBS (No. SH30071.03; Hyclone, GE Healthcare Biosciences). RPTECs were cultured in renal epithelial cell basal media supplemented with Renal Epithelial Cell Growth Kit (No. PCS-400–030, ATCC). NLFs were cultured in fibroblast basal medium supplemented with Low Serum Fibroblast Growth Kit (No. PCS-201–030, ATCC). HASMCs were grown in DMEM/F12 (1:1, Thermo Fisher Scientific) supplemented with 10% FBS and 1% penicillin/streptomycin (Thermo Fisher Scientific). Cell passages 1 to 3 maintained in culture at 37°C and 5% CO_2 were utilized for all experiments and where applicable, cells were serum starved using culture media supplemented with 0.1% FBS.

Lung tissue dissociation and primary cell culture

The use of human tissue samples complies with protocol No. AAAE9305 approved by the Institutional Review Board of Columbia University Medical Center in accordance with the Declaration of Helsinki ethical guidelines (23). Neoplastic pulmonary tissue was retrieved from a patient with LAM at the New York Presbyterian Hospital with informed written consent and placed in wash media containing DMEM/F12, 1% penicillin/streptomycin, and 3% FBS. The sample was processed within 30 to 60 minutes of biopsy as described (24). Cell suspensions were washed and then passed through a 40-μmol/L strainer, centrifuged at 400 × *g* for 10 minutes and pellets resuspended in complete DF8 culture media containing DMEM/F12, 10% FBS, 5×10^{-8} M sodium selenite (No. S521), 1.2×10^{-8} M vasopressin (No. V0377), 1×10^{-8} M cholesterol (No. C3045), 2×10^{-7} M hydrocortisone (No. H0888), 10 μg/mL transferrin (No. T1147), 1×10^{-9} M triiodothyronine (No. T6397), 0.025 mg/mL insulin (No. I6634), and freshly prepared 1.6×10^{-6}M ferrous sulfate (No. F8633; Sigma-Aldrich) for cell culture at 37°C and 5% CO_2. Passages 1 to 3 of these cells herein referred to as "pulmonary LAM tumor cells," were utilized for all experiments. Where applicable, pulmonary LAM tumor cells were serum starved using DF8 culture media supplemented with 0.1% FBS. DNA sequencing and alignment of pulmonary LAM tumor cell extracts with the 42 *TSC2* exons in chromosome 16 NC000016.10 (human reference genome GRCh38.p14) and tandem SNP mutational analysis revealed multiple bi-allelic frameshift and nonsense mutations particularly in *TSC2* exon 33 that leads to pathogenic mutations including p.L1480fs [dbSNP ID: rs45446594; SNP% = 29.16%) and p.Q1440fs (dbSNP ID: rs45517337; (SNP%) = 25%].

Cell survival assays

The pharmacologic effects of the TKI imatinib mesylate (Novartis) and the mTORC1 inhibitor rapamycin (LC Laboratories) on renal AML and pulmonary LAM tumor cell survival were assessed by both cell viability (CellTiter-Glo, No. G7571; Promega) and BrdU proliferation (No. 6813, Cell signaling Technology) assays. RPTECs and HASMCs were used in survival assays. Serum-starved renal AML cells, pulmonary LAM tumor cells, RPTECs, and HASMCs were incubated in 96-well plates (N = 2,500 cells/well, four wells per cell type per drug concentration) at 37°C for 24 hours with increasing concentrations of imatinib (0, 1, 5, and 10 μmol/L) and rapamycin (0, 0.0005, 0.05, and 1 μmol/L). Cultured cells were assayed for cell viability using the ATP-based CellTiter-Glo reagent luminescence assay, or for cell proliferation through their incorporation of 5-bromo-2′-deoxyuridine (BrdU) according to the manufacturers' instructions. Cell survival assays were repeated twice per cell type for each test and assessed in quadruplicate wells per drug concentration.

For Cilengitide (CGT) assays, both renal AML and pulmonary LAM tumor cells were preincubated overnight with 25 μmol/L small-molecule CGT (Catalog No. 22289; Cayman Chemicals), an antagonist of integrin (αIIbβ3) subreceptor ITGB3 (25) prior to drug induction experiments. These cells were compared with drug-induced neoplastic cells without CGT treatment. Thereafter, cell viability measurements were obtained using the CellTiter Glo viability assays as described above. CGT assays were repeated twice using three to four wells/drug concentration/experiment.

To inhibit inositol 1,4,5-triphosphate (IP_3)-induced calcium release from the endoplasmic reticulum of renal AML and pulmonary LAM tumor cells, one set of these cells were preincubated with 10 μmol/L cell-permeable allosteric inhibitor 2-aminoethyl diphenylborinate (2-APB; Catalog No. ab120124, Abcam) prior to drug induction (26). These cells were compared with drug-induced neoplastic cells without 2-APB treatment. Thereafter, cell viability measurements were obtained using the CellTiter Glo viability assays as described above. 2-APB assays were repeated twice using quadruplicate wells/drug concentration/experiment.

Flow cytometry

For the Annexin V-based apoptosis assay, drug-treated cells were incubated with TrypLE Express enzyme (Catalog No. 12604021; Thermo Fisher Scientific) for 8 minutes at 37°C and 5% CO_2, centrifuged, and washed with 1× Annexin V binding buffer. Thereafter, cells were incubated with Annexin conjugated to allophycocyanin (APC) fluorophore (660/20 nm) for 15 minutes (Catalog No. 88–8007–74, Thermo Fisher Scientific), followed by incubation with viability dyes propidium iodide (PI, 630/22 nm) or sytox green (SG, 530/30 nm) Thermofisher Scientific prior to flow cytometric analysis. Cells were gated for cell size and doublet cell exclusion by FSC-A / SSC-A and FSC-A / FSC-H respectively, followed by sorting for early-stage [APC(+); PI/SG(−)] versus late-stage [APC(+); PI/SG (+)] apoptosis on a Novocyte Quanteon cell analyzer (Agilent

Technologies). Unstained and single stained cells were used for compensation for each experiment. Experiments were performed using two to four biological replicates on different respective experimental days in technical duplicates per experiment.

IHC and immunocytochemistry

Four-μm-thick paraffin sections of human pulmonary LAM ($n = 6$) and healthy lung tissues ($n = 6$), invasive ductal carcinoma ($n = 2$), and colon cancer ($n = 2$) were obtained. Following antigen retrieval by autoclaving (121°C) for 20 minutes in pH 9.0 10 mmol/L Tris-HCl buffer, IHC was performed as previously described (27) using monoclonal rabbit anti-PDGFR-β (RRID:AB_1269704; No. ab69506) and anti-phospho-PDGFRβ (Y1021; RRID:AB_302554; No. ab16868; Abcam). Invasive ductal carcinoma and colon cancer tissue samples were used as positive controls for PDGFRβ and phospho-PDGFRβ reactivity respectively, whereas negative control slides were excluded from primary antibody staining.

For immunofluorescent staining of paraffin sections of imatinib-treated and PBS-treated renal cystadenomas, peroxidase activity was blocked in tumor sections following antigen retrieval with 6% hydrogen peroxidase for 10 minutes at room temperature. Tumor sections were incubated overnight at 4°C with rabbit monoclonal cleaved caspase-3 antibody (RRID:AB_2070042; Catalog No. 9664; Cell Signaling Technology) in the dark. Following washing, tumor sections were incubated with donkey anti-rabbit secondary antibody conjugated to Alexa Fluor 546 (RRID:AB_2534016; Catalog No. A10040, Thermo Fisher Scientific) prior to nuclear staining with Hoechst 33342 (Catalog No. 62249; Thermo Fisher Scientific). Immunofluorescent staining of renal angiomyolipoma 5-μm-thick ($n = 4$) frozen tissue sections and healthy renal tissue ($n = 5$) were similarly performed (without antigen retrieval) using rabbit monoclonal anti-PDGFR-β (RRID:AB_1269704; No. ab69506) and rabbit monoclonal anti-phospho-PDGFR-β (Y1021; Catalog No. 2227S, Cell Signaling Technology).

For immunocytochemistry, NLFs, pulmonary LAM tumor, and renal AML cells were cultured on cover slips (15 mm; Catalog No. 174969, Thermo Fisher Scientific), blocked and permeabilized, and incubated overnight at 4°C in the dark with mouse monoclonal anti-PDGFR-β (RRID:AB_1269704; No. ab69506) and anti-phospho-PDGFRβ (Y1021; RRID:AB_302554; No. ab16868; Abcam). After three washes, coverslips with cells were incubated with Alexa Fluor 488 fluorochrome-conjugated donkey-anti-rabbit secondary antibody (RRID:AB_2535792; Catalog No. A21206, Thermo Fisher Scientific) for 1 hour at room temperature, washed, and mounted on slides using DAPI-containing anti-fade mounting medium (Catalog No. P36971, Thermo Fisher Scientific). Hoechst 33342 (Thermofisher Scientific) was used for nuclear staining. Images were captured on a Ti Eclipse scanning confocal microscope with a Nikon A1 camera (Nikon Instruments Inc.). Immunostaining experiments were performed on duplicate slides/cell or tissue type/antibody using two different biological samples.

Western blotting

For protein blotting experiments of drug-treated cell lysates, nitrocellulose membranes were probed with the following primary antibodies to antigenic targets in the mTOR signaling pathways as described previously (27)—p70-s6 kinase (RRID:AB_331676; No. 9202S), anti-phospho-p70-s6 kinase (RRID:AB_330944; No. 9205S), anti-S6 ribosomal (RRID:AB_331355; No. 2217S), anti-phospho-S6 Ribosomal (RRID:AB_331682; No. 2215S), anti-ELF4B (RRID:AB_10698752; No. 3592), anti-phospho-ELF4B (RRID:AB_2097522; No. 3591S), anti-4EBP1 (RRID:AB_2097841; No. 9644S), anti-phospho-4EBP1 (RRID:AB_330985; No. 9459S), p62 (RRID:AB_10624872; No. 5114S), anti-phospho-AKT (Ser 473; RRID:AB_329825; No. 9271), anti-AKT (RRID:AB_329827; No. 9272; Cell Signaling Technologies), and anti–β-actin (RRID:AB_2223210; No. ab6276; Abcam).

Antibodies to PDGFR-β (RRID:AB_1269704; No. ab69506), phospho-PDGFRβ (Y1021; RRID:AB_302554; No. ab16868), and Cytochrome C (Catalog No. ab65311) were obtained from Abcam and also probed. Antibodies to inositol 1,4,5-triphosphate receptor (IP_3R) subtypes I, II, and III were obtained as a kind gift from Dr. Steve Marx (Division of Cardiology, Columbia University Medical Center). All membranes were washed with TBS-T, incubated with peroxidase (POD)-labeled secondary antibodies at room temperature, and visualized with Pierce ECL reagent (No. 32106, Thermo Fisher Scientific) and ImageQuant LAS 4000 Series imager (GE Healthcare Life Sciences). Where applicable, a single membrane was used to probe two to three antibodies and loading controls determined by differences in molecular weights of proteins being probed.

RT-qPCR, RNA sequencing, and IPA bioinformatics

Gene expression analysis by RT-qPCR was performed using primers for human *PTP4A3* (Hs02341135_m1), *INPP5D* (Hs00183290_m1), *MMP13* (Hs00233992_m1), *MTOR* (Hs00234508_m1), *DEPTOR* (Hs00961900_m1), and *ITGB3* (Hs01001469_m1; Catalog No. 4331182, Thermo Fisher Scientific) as described previously (27). Experiments were performed twice using two different biological samples.

Comparative RNA sequencing and Ingenuity pathway analysis of drug-induced renal AML cells and pulmonary LAM tumor cells was performed as described previously (28). Detailed procedures are also available in the supplementary text. Of interest to our study are resolved canonical signaling pathways and biofunctions between compared drug treatments that (i) vary widely in their predicted activation/inhibition (comparative *Z* scores) due to varying drug-type concentrations, and that (ii) exhibit significant *P* values for right-tailed Fisher exact tests establishing probabilistic fit between differentially expressed genes in our dataset and genes in the candidate canonical pathway or that necessitate the selected biofunction.

Cytochrome C release assay

Cytosolic and mitochondrial protein fractions of renal AML cells were prepared using the Cytochrome C releasing apoptosis assay kit (No. ab65311, Abcam) according to the manufacturer's protocol. Western blot band-integrated densities for cytochrome C in cell fractions were determined using the dot blot analysis protocol in ImageJ. Intensity ratios of organellar cytochrome C/β-actin protein bands were graphed to quantitatively normalize expression to a cellular endogenous protein.

Caspase activity assay

Detection of programmed cell death (apoptosis) in drug-treated cells was performed using the EnzChek Caspase 3-Assay Kit (Catalog No. E13184, Thermo Fisher Scientific) according to the manufacturer's protocol.

Animal studies

Animal drug study

Mice were maintained in the animal facility and genotyped using the *Tsc2* cDNA primer sequence: 5′-CAAACCCACCTCCTCAAGCTTC-3′ (forward) and 5′-AGACTGCCTTGGGAAAAGCG-3′ (reverse;

Integrated DNA Technologies, Research Triangle Park). In a randomized pilot study, two groups of six *Tsc2*$^{+/-}$ C57BL/6J mice littermates per group chosen randomly (RRID:IMSR_JAX:004686, male and female, 7 months old) were administered either imatinib (400 mg/kg/d) or PBS (200 μL) by oral gavage daily for 30 days. No local or systemic toxicity was observed in any of the animals following drug administration. Tumor volume measurements were determined at the beginning and end of experimentation using the VEVOLab 4.1 software provided by Visualsonics (FUJIFILM VisualSonics Inc.). After drug dosing, mice were sacrificed, and renal tumors excised and immediately washed in ice-cold PBS before flash freezing in liquid nitrogen. Approximately eight to 10 tumors/cysts were combined from each mouse for each Western blot experiment. Tumor samples were homogenized in bead-containing microfuge tubes containing fortified ice-cold RIPA buffer using a TissueLyser II (Qiagen) for 3 minutes at 30 Hz. Protein concentrations were determined using a BCA assay and gel separation, and antibody probing of 30 μg of loaded protein was performed as described in the Western blotting method section above. Probe antibodies include anti-Bcl-2 (RRID:AB_626736; Catalog No. sc-7382) and anti-Bad (RRID:AB_626717; Catalog No. sc-8044) mouse mAbs (Santa Cruz Biotechnology) and anti-Bax rabbit mAb (RRID:AB_725631; Catalog No. ab32503, Abcam)

Small animal ultrasound imaging

This technique was performed as previously described (29) at the Oncology Precision Therapeutic and Imaging Core (OPTIC) facility at the Columbia University Medical Center and used to monitor and measure tumor initiation and growth in the abdominal organs of 7-month-old *Tsc2*$^{+/-}$ mice.

Statistical analysis

Data collation and evaluation were performed using Microsoft Excel (v16.53) and statistical analysis was performed using Prism 9 (RRID: SCR_002798; v9.2.0, GraphPad Software). Sample sizes in experiments are specified in each figure legend and in the Materials and Methods section, and for all figures, statistical tests are appropriately justified. Data in the text and figures are expressed as mean ± SEM of multiple comparisons using either an ordinary one-way ANOVA or multiple *t* tests comparing two groups per drug concentration in CGT, 2-APB, and cell survival assays where $P < 0.05$ was considered statistically significant. Where applicable, *post hoc* Dunnett test for statistical significance against control/vehicle conditions was performed. Simple linear regression analysis was performed for caspase activity assays measuring significant differences between slopes of drug type-induced caspase activity per cell type over time. Linear equations and R^2 values are resolved, as well as *P* values computing results of an *F* test of the null hypothesis that slopes are zero (nonlinear) in a relationship between caspase activity and time. For apoptotic assays following cellular incubation with drugs, a two-way ANOVA with stage of apoptosis and drug condition as interacting factors and *post hoc* multiple comparisons using Dunnett tests for statistical significance against control/vehicle conditions for each apoptotic stage was performed.

In the randomized preclinical investigation to assess the phenotypic and molecular effects of imatinib administration *in vivo* in the *Tsc2*$^{+/-}$ mice as a pilot study, we employed a combination of the less rigorous resource equation method and power analysis approach (30). The power analysis demonstrates that the sample size of six mice per group (imatinib vs. PBS) has a 90% power to detect a 15% change in tumor count, tumor volume, or molecular expression between groups assuming a 5% significance level. Blinding was assured in this study as mouse genotyping, tumor detection, and 3D tumor volume determination was performed by independent laboratory technicians without knowledge of the hypothesis being tested. Inbred littermates were used in each mouse group, and mice were age- and sex-matched for each group. Mouse littermates were also selected for the imatinib or PBS group at random.

Study approval

All animal experimentation was approved by the Institutional Animal Care and Use Committee (IACUC) at Columbia University Medical Center under protocol No. AC-AABF2559. The use of human tissue samples is in compliance with protocol No. AAAE9305 and was performed in accordance with the Declaration of Helsinki (23) ethical guidelines and approved by the Institutional Review Board of Columbia University Medical Center. Informed written consent was received from patients prior to participation.

Data availability

The raw datasets generated and analyzed for RNA sequence analysis of renal angiomyolipoma cells and pulmonary lymphangioleiomyomatosis tumor cells have been deposited in NCBI GeoDataset as GSE193402 and GSE193398, respectively.

Results

Mesenchymal lineage marker PDGFRβ is exclusively activated in LAM and AML tumors

Expression of both PDGFRβ and its activated form in human renal AML tumor slices (Supplementary Figs. S1A and S1C) and LAM pulmonary tumor slices (Supplementary Figs. S1E and S1G) by IHC was resolved. Age-matched normal renal tissue slices expressed the PDGFRβ receptor (Supplementary Fig. S1D) but not phospho-PDGFRβ (Supplementary Fig. S1B), distinguishing renal tumorigenic tissue states from normal (31). Neither the expression of PDGFRβ receptor nor its phosphorylated form was observed in healthy lung tissue (Supplementary Figs. S1F and S1H). This result was extended to the cellular level where the expression of phospho-PDGFRβ was also not observed in normal human lung fibroblasts (Supplementary Fig. S1M). Both dissociated patient-derived LAM pulmonary tumor cells (Supplementary Fig. S1N) and UMB1949 renal AML cells (Supplementary Fig. S1O) expressed the activated form of the tyrosine receptor kinase, respectively.

Receptor tyrosine kinase inhibition yields significantly higher tumoricidal potential in pulmonary LAM and renal angiomyolipoma cells

The effects of the TKI imatinib on representative UMB 1949 renal AML and patient pulmonary LAM tumor cell survival was then compared with the effect of rapamycin. Rapamycin at all concentrations (0.0005–1 μmol/L) significantly decreased proliferation of both RPTECs (*, $P < 0.05$) and renal angiomyolipoma cells (AMLs; *, $P < 0.001$) compared with nontreated control cells (**Fig. 1A**). A concentration-specific effect was observed when these cells were exposed to the TKI imatinib (10 μmol/L), which also significantly reduced renal AML cell proliferation by 20% compared with its effect on nontumor RPTECs ($^{\Phi}P < 0.05$; **Fig. 1B**). Rapamycin (**Fig. 1C**), imatinib (**Fig. 1D**), and nilotinib (Supplementary Fig. S2A) decreased proliferation of both control HASMCs and pulmonary LAM tumor cells at similar rates (*, $P < 0.05$; $^{\#}$, $P < 0.05$). Nilotinib as a second-generation TKI (0.0005–0.05 μmol/L) did not differentially decrease renal AML cell proliferation compared with proliferation of RPTECs (Supplementary Fig. S2C).

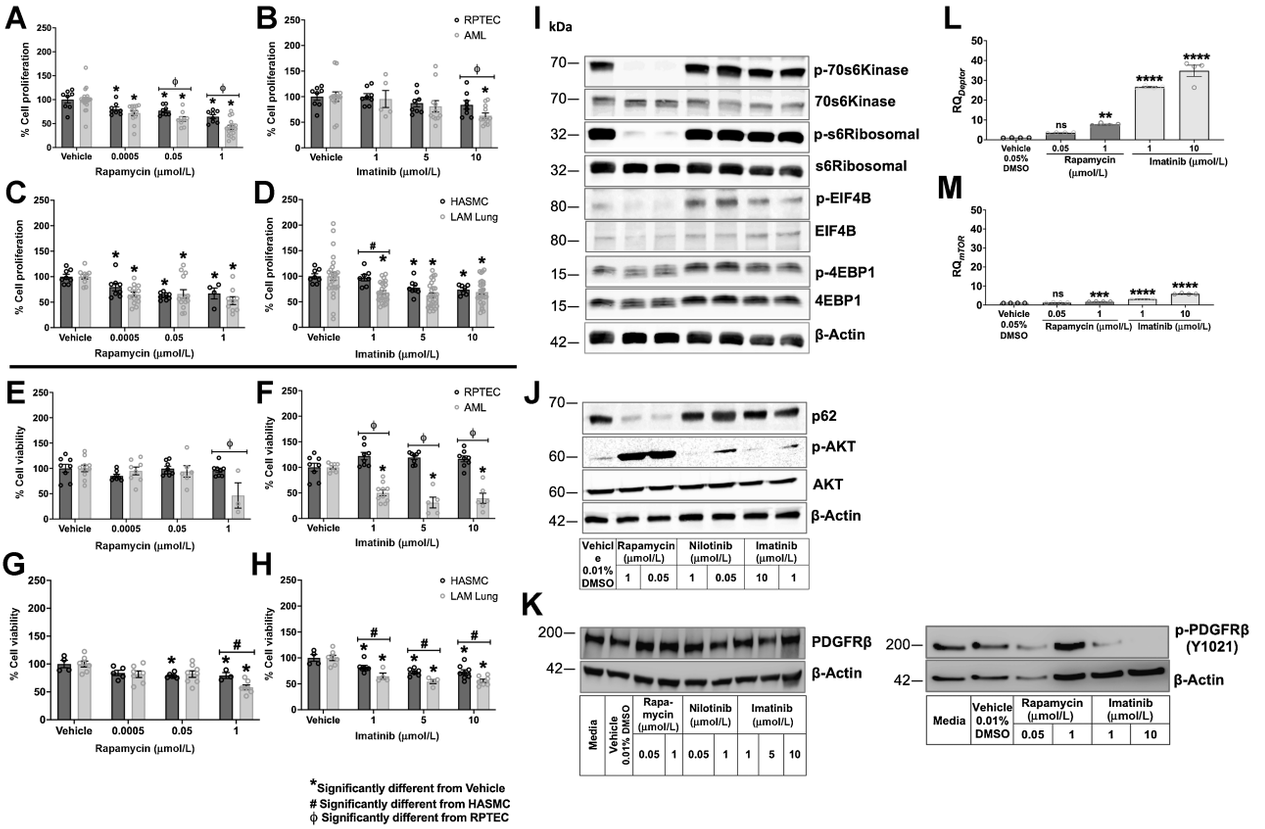

Figure 1.

TKIs limit survival of UMB1949 renal angiomyolipoma and pulmonary LAM tumor cells via PDGF signaling. The cytocidal properties of imatinib and rapamycin on renal angiomyolipoma and pulmonary LAM tumor cells were compared by assessing drug effects on both cell proliferation and viability over 24 hours using BrdU and ATP-based luminescence cell viability assays, respectively. Rapamycin exhibited robust inhibition of cell proliferation at all concentrations tested (0.0005–1 μmol/L) in both UMB1949 renal AML (**A**) and pulmonary LAM primary tumor cells (**C**) and in their respective control cells, RPTECs, and airway smooth muscle cells (HASMCs) albeit at slightly lower inhibition rates (*, $P < 0.05$; ϕ, $P < 0.05$). **B,** Imatinib was selectively cytostatic to renal AMLs at 10-μmol/L concentration compared with RPTECs (*, $P < 0.05$; ϕ, $P < 0.05$) and equally reduced proliferation rates of LAM tumor cells and HASMCs by up to 30% at highest concentration of 10 μmol/L assessed (*, $P < 0.05$; #, $P < 0.05$; **D**). Both renal AML (**E**) and pulmonary LAM tumor cell viability (**G**) were significantly reduced only at cytotoxic rapamycin concentration of 1 μmol/L compared with RPTECs and HASMCs (*, $P < 0.05$; ϕ, $P < 0.05$; #, $P < 0.05$). **F** and **H,** Imatinib exhibited significant cytocidal effects on both renal AMLs and pulmonary LAM tumor cells at all concentrations tested and significantly reduced their viability compared to RPTECs and HASMCs (*, $P < 0.05$; ϕ, $P < 0.001$; #, $P < 0.05$). Vehicle denotes 0.01% dimethylsulfoxide (DMSO) in respective culture media. Experiments were repeated twice using four wells/drug concentration/experiment. Error bars denote mean ± SEM of replicate experiments assessed for statistical significance using multiple *t* tests comparing test wells to vehicle, between UMB1949 renal AMLs and RPTECs and between LAM tumor cells and HASMCs. **I,** Immunoblots of lysates from drug-induced renal AML cells showing reactivity to antibodies and phospho-antibodies against downstream mTOR pathway targets: 70s6 kinase, s6 ribosomal, elf4b, and 4ebp1. AML cells were exposed to high and low concentrations of rapamycin, imatinib, and analogous TKI nilotinib, for 24 hours under serum starvation conditions. **J,** Renal AML cells selectively exhibit rapamycin-induced p62 downregulation and elevated phospho-Akt at Ser473, indicative of sustained cell proliferation and survivability compared with cells exposed to tyrosine kinase inhibitors imatinib and nilotinib. **K,** Western blots reveal that the TKI imatinib selectively induced a dose-dependent inactivation of PDGFRβ in renal AML cells at concentrations of 1 to 10 μmol/L coincident with the drug's increasing cytocidal effect on tumor cells. The expression of *MTOR* (**L**) and *DEPTOR* (**M**) components of the *mTORC1* complex assessed by RT-qPCR significantly increased in renal AML cells treated with increasing imatinib concentration from 1 to 10 μmol/L and toxic rapamycin concentration (1 μmol/L).

Importantly, although physiologic concentrations of rapamycin did not affect the viability of RPTECs and renal AMLs (**Fig. 1E**), imatinib caused a 40% to 70% decrease in the viability of renal AML cells (*, $P < 0.0001$; **Fig. 1F**) in a dose-dependent manner compared with culture conditions containing no drug. Rapamycin also only significantly decreased pulmonary LAM tumor cell viability at toxic concentrations (1 μmol/L; *, $P < 0.05$; ϕ, $P < 0.05$; #, $P < 0.05$; **Fig. 1G**), whereby 10 μmol/L imatinib caused a 25% to 40% decrease in viability of pulmonary LAM tumor cells (*, $P < 0.001$; **Fig. 1H**). Imatinib exerted significantly greater cytocidal effects in renal AMLs (**Fig. 1F**) and pulmonary LAM tumor cells (**Fig. 1H**) compared with their respective RPTEC ($^{\phi}P < 0.001$) and HASMCs ($^{\#}0.05 < P < 0.005$) control cells. Nilotinib yielded similar results exhibiting the most robust cytocidal activity against renal AML cells (0.0005–1 μmol/L, *, $P < 0.05$; Supplementary Fig. S2D).

Attenuation of renal AML cell survival by TKIs occurs via the PDGF pathway

mTOR signaling was then examined in tumor cells treated with TKIs and rapamycin. *TSC2* mutations typically activate Rheb GTPase, which relieves inhibition of mTORC1 resulting in high basal levels of phospho-S6 kinase and phospho-S6 ribosomal (32). Imatinib and

nilotinib both elicited dephosphorylation of Akt in renal AMLs and attenuation of renal AML cell survival without affecting candidate downstream signaling targets of the mTOR pathway or p62 (**Fig. 1I** and **J**). As expected, protein blots of renal AML cells exposed to varying drug concentrations of 0.05 and 1 μmol/L rapamycin revealed complete dephosphorylation of s6 kinase at T389, EIF4B at S422, and of both s6 ribosomal at S240/244 and 4EBP1 at T37/46 (**Fig. 1I**) signaling successful inhibition of mTOR pathway activity. Rapamycin-induced inactivation of mTORC1 also dramatically reduced autophagy adapter p62 levels in a dose-dependent manner (33) and activated protein kinase B (Akt; **Fig. 1J**). TKIs nilotinib and imatinib also induced a dose-dependent inhibition of PDGFRβ activation in renal AML cells from 0.05 to 1 μmol/L and from 1 to 10 μmol/L concentrations respectively by protein blotting, coincident with the drugs' increasing cytocidal effect on tumor cells (**Fig. 1K**). This protein expression pattern was not observed in lysates of rapamycin-treated renal AML cells and directly implicates PDGF signaling in TKI-induced cytocidal activity in renal AML cells. Furthermore, gene expression of *MTOR* (**Fig. 1L**) and *DEPTOR* (**Fig. 1M**) components of the *mTORC1* complex assessed by RT-qPCR significantly increased in renal AML cells treated with imatinib concentrations 1 to 10 μmol/L [and toxic rapamycin concentration (1 μmol/L)] compared with physiologic rapamycin concentration (0.05 μmol/L), supporting our findings that the mTOR pathway is not directly involved in the cytocidal mechanisms of TKIs.

GPVI signaling and G_2–M cell-cycle regulation distinguishes imatinib-based tumoricidal mechanisms in renal AMLs and pulmonary LAM tumor cells

To discern signaling pathways that illuminate differences between rapamycin-induced versus imatinib-induced renal AML cells, RNA sequencing and bioinformatic analysis of RNA isolates from drug-induced cells was performed. The results of IPA comparison analysis mapping renal AML genes differentially expressed upon drug treatment are displayed revealing the top 20 canonical pathways (**Fig. 2A**) and diseases/biofunctions (**Fig. 2B**) to which the genes and their pathway regulators are most closely associated by significant *z*-scores. Results of Fisher exact tests of association also support the findings that the differentially expressed renal AML genes did associate with select IPA canonical pathways (Supplementary Fig. S3A) and biofunctions (Supplementary Fig. S3B) by significant *P* values. Notable signaling pathways with drug type concentrations yielding both significant *z*-scores and *P* values include IL6 signaling, HMGB1 signaling, cholecystokinin/gastrin-mediated signaling, peroxisome proliferator-activated receptor (PPAR) signaling, and GPVI signaling pathways (**Fig. 2A**). Of these biochemical mechanisms, only the GPVI pathway is predicted to be activated in rapamycin-induced renal AML cells (0.05 μmol/L; $Z = 2.673$; $P = 1.96\text{E}{-03}$) but inhibited in renal AML cells exposed to imatinib (10 μmol/L; $Z = -2.12$; $P = 0.01$). This observation constitutes widely varying activation/inhibition states upon differential drug induction at physiologically relevant concentrations of rapamycin (**Fig. 1A** and **E**) versus imatinib (**Fig. 1B** and **F**), and the GPVI pathway is thus likely central to distinguishing drug-type signaling effects on renal AML cells.

Using the same selection criteria, genes defined by IPA to be associated with curated diseases and biological functions were compared in rapamycin- and imatinib-treated renal AML cells and ranked (**Fig. 2B**). Depending on drug type and concentration, gene expression varied widely specifically in cell survival [(rapamycin: 0.05 μmol/L; $Z = -1.1$; $P = 4.21\text{E}{-06}$), (imatinib: 10 μmol/L; $Z = -2.79$; $P = 8.66\text{E}{-05}$)] and cell viability [(rapamycin: 0.05 μmol/L; $Z = -0.83$; $P = 1.14\text{E}{-05}$), (imatinib: 10 μmol/L: $Z = -2.4$; $P = 1.9\text{E}{-04}$)] functions. Supplementary Table S1 reveals candidate cell survival and viability genes with the most contrasting expression states in rapamycin-induced versus imatinib-induced renal AML cells and represent gene expression states likely central to distinguishing signaling pathways of imatinib. Compared with rapamycin exposure, renal AML cells exposed to imatinib induced significant downregulation/repression of genes involved in cancer cell proliferation, survival, and metastasis, and stimulated tumor cell apoptosis by statistically significant repression of inositol polyphosphate-5-phosphatase D (*INPP5D*; ref. 34), *MYC* proto-oncogene (35), protein tyrosine kinase beta (*PTK2B*; ref. 36), *STAT5A* (37), and induced tumor angiogenesis by downregulating matrix metalloproteinase 13 *(MMP13*; ref. 38; Supplementary Table S1). The expression of several of these genes was validated by RT-qPCR and confirmed statistically significant downregulation of *PTP4A3* ($P < 0.0001$; **Fig. 2C**), *INPP5D* ($P = 0.0004$; $P < 0.0001$; **Fig. 2D**), and *MMP13* ($P < 0.005$; $P < 0.005$; **Fig. 2E**) in imatinib-induced renal AML cells (10 μmol/L) compared with cells not exposed to drugs and those exposed to rapamycin (0.05 μmol/L), respectively.

Fewer canonical pathways and biofunctions differed between rapamycin and imatinib-induced pulmonary LAM tumor cells possibly due to the heterogeneity of the primary pulmonary LAM tumor cell phenotype (8). Importantly, the cell-cycle G_2–M DNA damage checkpoint regulation pathway was not affected by imatinib (10 μmol/L; $Z = 1.0$; $P = 2.2\text{E}{-03}$) but was differentially activated in pulmonary LAM tumor cells treated with rapamycin (0.05 μmol/L; $Z = 2.11$; $P = 2.88\text{E}{-07}$; **Fig. 2F**; Supplementary Fig. S4A). Imatinib also significantly downregulated PDGF signaling (10 μmol/L; $Z = -2.236$; $P = 2.38\text{E}{-02}$) in pulmonary LAM tumor cells compared with rapamycin (0.05 μmol/L; $Z = -1.134$; $P = 0.054$; **Fig. 2F**; Supplementary Fig. S4A), and thus abolished the tumorigenic mesenchymal phenotype, possibly interfering with EMT and tumor progression (39).

The stark distinction in gene expression patterns between rapamycin and imatinib-induced renal AML cells (**Fig. 2G**) and pulmonary LAM tumor cells (**Fig. 2H**) can be further visualized in principal component analyses (PCA) plots, which cluster RNA sequence data based on drug type. In renal AML cells, variances in gene expression patterns were resolved with the first eigenvalue of 0.60 distinguishing rapamycin-induced renal AML cells from cells induced by imatinib (**Fig. 2G**), indicating differential drug-induction mechanisms. The second eigenvector (PC2 = 0.30) seemed to account for genetic variances due to drug induction compared to noninduced renal AMLs. The heterogeneity of the pulmonary LAM cell is reflected in its relevant PCA plot, where the first eigenvector (PC1 = 0.61) differentiated drug-type concentrations eliciting significant cellular genetic responses including cytocidal 10 μmol/L imatinib, cytotoxic 1 μmol/L rapamycin and cytostatic 0.05 μmol/L rapamycin, versus those exhibiting relatively quiescent genotypic signatures in pulmonary LAM tumor cells (**Fig. 2H**). The second eigenvector (PC2 = 0.15) distinguished between rapamycin versus imatinib-induction of pulmonary LAM tumor cells but suggests that differential drug induction accounts for only 15% of the variability in gene expression observed in this neoplastic cell type (**Fig. 2H**).

Differential ER-based IP_3 receptor-type signaling underlies imatinib-induced apoptosis in renal AML and pulmonary LAM tumor cells

In validating the role of the GPVI signaling pathway resolved by IPA bioinformatics (**Fig. 2A**), the "inside-out" activation of the integrin

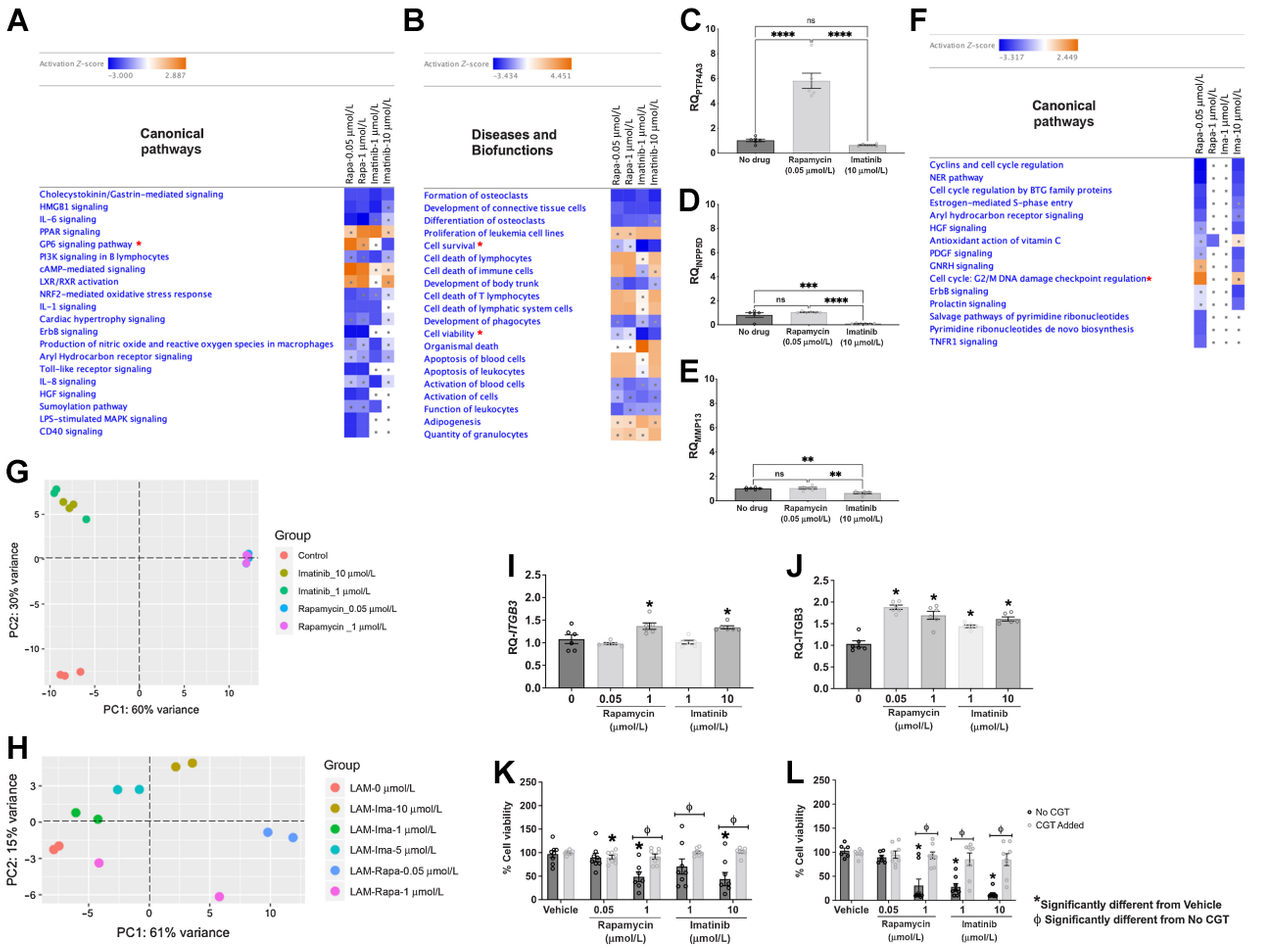

Figure 2.

Differential signaling mechanisms induced by rapamycin compared to imatinib in UMB1949 renal angiomyolipoma and pulmonary LAM tumor cells. Top 20 canonical signaling mechanisms (**A**) and biological functions (**B**) predicted to be activated (*Z*-score ≥ 2, orange squares) or inhibited (*Z*-score ≤ −2, blue squares) by concentrations of rapamycin or the TKI imatinib determined by comparative RNA-sequencing analysis. GPVI signaling and cell survival and viability biofunctions (indicated with red asterisks) were resolved canonical pathways and biofunctions that exhibit both widely varying significant *Z*-scores by drug type and significant *P* values of Fisher exact tests of the likelihood of association of differentially expressed genes in our dataset with curated genes and canonical pathways in IPA knowledge base (see Supplementary Figs. S3A and S3B). RT-qPCR validation of cell survival and viability genes resolved by IPA bioinformatics including (**C**) protein tyrosine phosphatase type A3 (*PTP4A3*), (**D**) inositol polyphosphate-5-phosphatase D (*INPP5D*), and (**E**) matrix metalloproteinase 13 (*MMP13*) was performed. Experiments were run in quadruplicates per gene per sample and $N = 2$ biological samples were used for RT-qPCR analysis. Statistical comparisons were performed using a one-way ANOVA with *post hoc* Dunnett multiple comparisons test where **, $P < 0.005$, ***, $P = 0.0006$, ****, $P < 0.0001$; and ns, not significant. **F,** Bioinformatics analysis of differentially expressed genes when pulmonary LAM is treated with rapamycin versus imatinib reveals activation of G_2–M cell-cycle regulatory mechanisms only in 0.05 µmol/L rapamycin condition. RNA sequencing was performed using ($N = 3$) biological replicates of renal AML and ($N = 2$) pulmonary LAM cell lysates. Gray dots denote test conditions resulting in nonsignificant values below set threshold ($-2 \geq Z \geq 2$). Principal component analysis cluster renal AML RNA sequence data by drug type (**G**) with variances resolved with first eigenvalue of 0.60, and cluster pulmonary LAM tumor cells (**H**) with first eigenvalue of 0.61 indicating differential drug-induction mechanisms in these cells. Integrin subunit beta 3 (*ITGB3*) is significantly upregulated in renal AML cells exposed to 1 µmol/L Rapamycin (*, $P < 0.01$) and 10 µmol/L imatinib (*, $P < 0.05$; **I**) and at all concentrations in pulmonary LAM cells (*, $P < 0.001$) by RT-qPCR (**J**). Pharmacologic inhibition of ITGB3 in renal AML cells (*, $0.05 > P < 0.001$; ϕ, $0.05 > P < 2.4E{-}05$; **K**) and pulmonary LAM tumor cells (*, $0.0005 > P < 7.23E{-}07$; ϕ, $1.9E{-}05 > P < 1.0E{-}0.6$; **L**) using small molecule CGT at 25 µmol/L concentration significantly reversed cytotoxicity of 1 µmol/L rapamycin and cytocidal effects of 1 and 10 µmol/L imatinib compared with experimental conditions where CGT was not added. RT-qPCR experiments were performed twice using three wells/concentration/experiment. CGT assays were performed twice using three to four wells/concentration/experiment. Error bars denote mean ± SEM of replicate experiments assessed for statistical significance using a one-way ANOVA with *post hoc* Dunnett multiple comparisons test (RT-qPCR) or multiple *T* tests (CGT assays). Vehicle = 0.01% DMSO in respective cell culture media.

(αIIbβ3) subreceptor ITGB3 in the GPVI pathway in renal AML cells was modulated utilizing the small molecule inhibitor CGT. This ITGB3 coreceptor has been associated with epithelial-to-mesenchymal transitions and tumor metastasis (40), and our findings reveal significant upregulation of the *ITGB3* gene in renal AML cells exposed to cytotoxic 1 µmol/L rapamycin ($P < 0.01$), cytocidal 10 µmol/L imatinib ($P < 0.05$; **Fig. 2I**), and to all drug concentrations in pulmonary LAM neoplastic cells ($P < 0.001$; **Fig. 2J**). We hypothesized that CGT, a synthetic cyclic RGD-containing peptide with high affinity for class αVβ3 and αVβ5 integrins and anti-invasive properties in

certain cancer types (25) would reverse drug effects on tumor cell viability, indicative of active GPVI pathway signaling. As hypothesized, CGT (25 μmol/L) significantly eliminated the cytotoxic effects of 1 μmol/L rapamycin and cytocidal effects of imatinib (1 μmol/L, 10 μmol/L) in both renal AML cells ($0.05 > P < 0.001$; $^{\Phi}0.05 > P < 2.4E{-}05$; **Fig. 2K**) and pulmonary LAM tumor cells ($0.0005 > P < 7.23E{-}07$; $^{\Phi}1.9E{-}05 > P < 1.0E{-}0.6$; **Fig. 2L**) compared with experimental conditions where CGT was not added. These results annotated the potential role of GPVI pathway signaling in drug-induced cytocidal events of both renal AML and pulmonary LAM tumor cells.

The GPVI pathway gene expression states in our datasets was then compared with the expected expression state of the genes when the GPVI canonical pathway is activated or inhibited as curated by ingenuity pathway analysis (IPA). The comparative bioinformatics analysis predicts that ultimately, inositol IP_3 product of phosphatidylinositol 4,5-diphosphate (PIP2) cleavage interacts with Ca^{2+} ionophores in the endoplasmic reticulum (ER) of both renal AML cells (**Fig. 3A**) and pulmonary LAM tumor cells (**Fig. 3B**) exposed to 10μmol/L imatinib to trigger Ca^{2+} release from ER stores into the cytoplasm (demarcated in purple squares). This pathway activity is an established tumoricidal event (41) not predicted to occur in renal AML cells (**Fig. 3C**) or pulmonary LAM tumor cells (**Fig. 3D**) exposed to cytostatic rapamycin (0.05 μmol/L; demarcated in purple squares). These results implicate calcium efflux mechanisms via regulated ER-based IP_3 receptors as key to the cytocidal capacity of imatinib in both renal AMLs and pulmonary LAM tumor cells. Protein expression studies of IP_3 receptor subtypes in both drug-induced renal AML (**Fig. 3E**) and pulmonary LAM neoplastic cells (**Fig. 3F**) validates the bioinformatic prediction by revealing a dose-dependent molecular switch from inositol IP_3R subtype I to subtype III unique to increasing imatinib concentrations from 1 to 10 μmol/L. These higher imatinib doses were significantly cytocidal to renal AML and pulmonary LAM tumor cells (**Fig. 1F** and **H**), suggesting that IP_3 receptor switching could modulate ER calcium effluxes that are tumoricidal.

In further validation studies, the effects of IP_3R-induced calcium efflux on tumor cell viability following drug treatment were investigated. The renal AML and pulmonary LAM tumor cells were incubated overnight with 10 μmol/L cell-permeable 2-aminoethyl diphenylborinate (2-APB), an effective blocker of IP_3-induced calcium release from the ER (26). After tumor cell exposure to imatinib, results depicted in **Fig. 3G** reveal that 2-APB administration blocked the cytocidal effect of imatinib (1–10 μmol/L) in renal AML cells by 15% to 30% ($^{*}0.05 > P < 0.003$; $^{\Phi}0.02 > P < 1.0E{-}06$) compared with cell culture conditions with no 2-APB added. Pulmonary LAM tumor cells preincubated with 2-APB prior to drug induction were also protected from cytocidal effects of imatinib ($^{*}0.005 > P < 1.17E{-}07$; $^{\Phi}P < 1.0E{-}06$; **Fig. 3H**). These results confirm that IP_3R-induced calcium efflux is a defining cytocidal mechanism induced by imatinib in both tumor cell types.

To examine the effect of fluxes in IP_3R isoform-type signaling on mitochondrial and cytoplasmic cytochrome C levels in drug-treated renal AML cells, cytochrome C assays were performed. Results reveal increasing mitochondrial cytochrome C (**Fig. 4A** and **B**) with concomitant decrease in cytosolic cytochrome C (**Fig. 4A** and **C**) upon induction of renal AMLs with increasing concentrations of rapamycin (0.05–1 μmol/L). Conversely, mitochondrial cytochrome C levels in these cells reduced upon treatment with increasing imatinib concentrations from 1 to 10 μmol/L (**Fig. 4A** and **B**), whereas cytosolic cytochrome C increased (*, $P < 0.05$) in cell cultures treated with 10 μmol/L imatinib compared with nontreated control cells (**Fig. 4A** and **C**). These drug-induced cytochrome C fluxes were not observable in renal AML whole cell lysates (Supplementary Fig. S5). To determine whether the observed drug-induced organellar cytochrome C fluxes translated to the proapoptotic induction of caspase activity, a caspase 3/7 activity assay was performed over a 6-hour period following drug treatment of renal AML cells. Simple linear regression analyses results revealed a statistically significant increase in caspase activity beginning at the 5-hour timepoint and exclusive to only renal AMLs treated with cytocidal 10 μmol/L imatinib ($y = 2760x{-}13625$; R2 = 0.95; *, $P < 0.0001$, $N = 2$; **Fig. 4D**). These results suggest that differential ER calcium efflux specifically triggered by 10 μmol/L imatinib suffices to stimulate mitochondrial-mediated apoptosis in renal AML cells, establishing the cytocidal mechanism of this TKI concentration.

Next, we performed annexin-V–based assay on the drug-treated renal AML cells and control RPTECs, and pulmonary LAM tumor cells and control HASMCs to confirm our findings that TKI concentrations induce apoptosis in neoplastic cells used in this study. This assay distinguishes early-stage apoptotic cells [fluorophore-conjugated Annexin V (+), viability dye (-)] from late-stage apoptotic cells [fluorophore-conjugated Annexin V (+), viability dye (+)] cells by flow cytometric cell sorting (42). **Figure 5A** displays the gating scheme used to ascertain the proportion of early-stage and late-stage apoptotic cells caused by 24-hour incubation with select imatinib versus rapamycin concentrations. Experimental results displayed in **Fig. 5B** to **D** (and Supplementary Table S2) indicates that imatinib (10 μmol/L) exclusively induced significantly higher proportions of early-stage apoptotic ($39.6 \pm 1.34\%$ SEM; ****, $P < 0.0001$; $N = 8$) and late-stage apoptotic ($19.1 \pm 2.94\%$ SEM; ****, $P < 0.0001$; $N = 8$) renal AML cells but did not significantly induce apoptosis compared with control conditions in other cell types.

Imatinib administration stunts renal tumor growth in the $tsc2^{+/-}$ mice

A preclinical study to test the efficacy of imatinib in ameliorating tumor incidence and growth *in vivo* was subsequently performed using an established haploinsufficient $Tsc2^{+/-}$ mouse model of TSC. In these mice, the spontaneous onset of solid renal tumors and fluid-filled renal cysts (**Fig. 6A**) was detected beginning at 4 months of age, and tumor development was noninvasively tracked using high-frequency ultrasound imaging (**Fig. 6B**–**E**). At the 7-month timepoint, imatinib (400 mg/kg/d, $N = 6$ mice) or PBS ($N = 6$ mice) was administered in the $Tsc2^{+/-}$ mice by oral gavage for 30 days after which changes in tumor volumes were determined. Representative ultrasound images of tumor tracking before and after drug administration in the imatinib-treated mice study group (**Fig. 6B** and **D**) and PBS mice group (**Fig. 6C** and **E**) respectively are provided. Results displayed in **Fig. 6F** and Supplementary Table S3 reveal that imatinib significantly decreased the volume of renal tumors (**, $P = 0.001$; $N = 10$ tumors) detected at the beginning of the study by an average of 45.15% from an aggregate volume of 141.2 to 127.23 mm^3 compared with age-matched PBS-treated littermates in which renal cystadenomas ($N = 5$ tumors) increased by over 200% from an aggregate volume of 2.09 to 9.26 mm^3 over the same 30-day treatment period. Analogous results were obtained when mean tumor areas were calculated in formalin-fixed paraffin-embedded serial sections (4 μmol/L) of renal cystadenomas obtained from PBS-treated ($N = 3$ mice) versus imatinib-treated ($N = 3$ mice) $Tsc2^{+/-}$ mice after the 30-day drug study similar to previously described methods (43). In this analysis, equal cross-sectional areas of seven to eight regions of dysmorphic tissue/section were determined for six tumor sections/drug treatment. Results revealed that mean ± SEM of renal tumor area in histologic

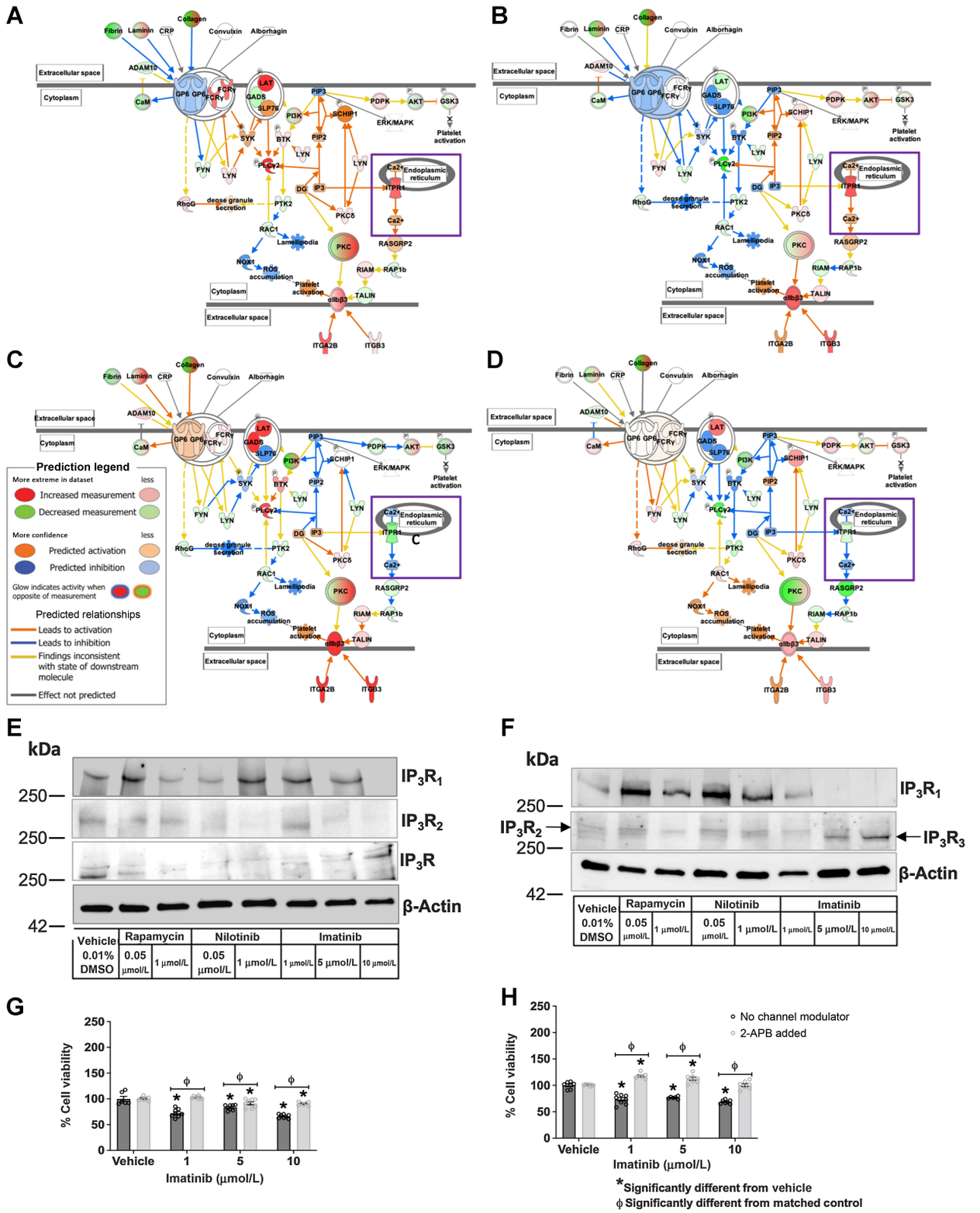
A
B
C
D
Extracellular space
Cytoplasm
Collagen
Fibrin
Laminin
CRP
Convulxin
Alborhagin
ADAM10
CaM
GP6
FCRγ
LAT
GADS
SLP76
PI3K
PIP3
SCHIP1
PDPK
AKT
GSK3
ERK/MAPK
Platelet activation
SYK
BTK
PIP2
LYN
FYN
PLCγ2
DG
IP3
Ca2+
Endoplasmic reticulum
ITPR1
RhoG
dense granule secretion
PTK2
PKCδ
RAC1
Lamellipodia
PKC
RASGRP2
NOX1
ROS accumulation
RIAM
RAP1b
TALIN
αIIbβ3
ITGA2B
ITGB3
Prediction legend
More extreme in dataset
less
Increased measurement
Decreased measurement
More confidence
Predicted activation
Predicted inhibition
Glow indicates activity when opposite of measurement
Predicted relationships
Leads to activation
Leads to inhibition
Findings inconsistent with state of downstream molecule
Effect not predicted
E
kDa
250
IP3R1
IP3R2
IP3R
β-Actin
42
Vehicle 0.01% DMSO
Rapamycin 0.05 μmol/L
1 μmol/L
Nilotinib 0.05 μmol/L
1 μmol/L
Imatinib 1 μmol/L
5 μmol/L
10 μmol/L
F
IP3R3
G
% Cell viability
Imatinib (μmol/L)
H
No channel modulator
2-APB added
*Significantly different from vehicle
ϕ Significantly different from matched control

sections of imatinib-treated mice ($4.61 \times 10^4 \pm 2904\ \mu m^2$) was significantly less than mean neoplastic area in histologic renal tumor sections obtained from PBS-treated mice ($8.03 \times 10^4 \pm 2956\ \mu m^2$) calculated using an unpaired T test ($N = 47$ tumor areas/drug treatment; ****, $P < 0.0001$) (**Fig. 6G**).

In imatinib-treated mice, five new tumors with mean volume measurement of $0.218 \pm 0.06\ mm^3$ developed between six mice (M1–M6), whereas three new tumors with mean volume measurement of $0.50 \pm 0.37\ mm^3$ developed in the PBS treatment mice group (M1–M6; Unpaired t test: $P = 0.35$; **Fig. 6H**; Supplementary Table S3). Lysates of renal tumors/cysts and adjacent nontumorigenic renal tissue from imatinib and PBS-treated mice were assayed to ascertain the expression of canonical apoptotic markers. Results displayed in **Fig. 6I** reveal selective expression of apoptosis regulators *Bcl-2*, Bcl-2-associated X (*Bax*), and Bcl-2-associated agonist of cell death (*Bad*) only in renal cysts and tumors treated with imatinib compared with adjacent normal renal tissue and renal tumors in the PBS mice group. We also compared expression of cleaved caspase-3, an apoptosis marker, on formalin-fixed paraffin-embedded sections (4 μmol/L) of renal cystadenomas obtained from PBS-treated ($N =$ versus imatinib-treated $Tsc2^{+/-}$ mice after the 30-day drug study period. Results depicted in **Fig. 6J–L** show no positive staining for anti-cleaved caspase-3 antibodies in renal tumor sections obtained from PBS-treated $Tsc2^{+/-}$ mice but robust expression of cleaved caspase-3 in renal tumor sections obtained from imatinib-treated $Tsc2^{+/-}$ mice (**Fig. 6M–O**).

Discussion

In this study, the therapeutic potential of inhibiting receptor tyrosine kinases in mesenchymal tumor lineages in TSC and LAM was explored. These compounds exhibited over 25% higher cytocidal effects on renal angiomyolipoma and pulmonary LAM neoplastic growth than the current FDA-approved rapamycin-based therapy with minimal toxic effects on resident healthy cells. Additionally, TKIs were shown to induce molecular signaling leading to apoptosis in a concentration-dependent manner in cell culture and animal model systems. Most importantly, these inhibitors exert their effects on TSC and LAM neoplasms via the PDGF pathway whose biological signaling targets have been resolved, and thus can be further manipulated for novel therapies and better clinical outcomes. The selective activation of canonical mesenchymal lineage marker platelet-derived growth factor receptor β (PDGFRβ) in renal AML and pulmonary LAM tumorigenic tissues and cells translates the studies into the therapeutic arena as we have shown that LAM and TSC can be derived from neural crest cells that ontogenetically give rise to pathogenic mesenchymal tumors (29). Therefore, use of the pharmacological inhibitors of PDGFR activation is a logical therapeutic approach to this disease and may be a potential treatment for other similar tumor malignancies.

The present studies reveal that inhibiting PDGFRβ activation using TKIs significantly reduced renal AML cell survival without affecting the expression of downstream targets of the mTOR pathway. These inhibitors also did not affect p62 expression in renal AML cells that might indicate that stress-induced autophagic processes that typically provide anabolic building blocks and intracellular energy sources to sustain tumor cell survival could be inactivated (44). Mechanistically, serine/threonine kinase Akt (protein kinase B) de-phosphorylation at Ser473 observed in imatinib-treated renal AML cells occurred in a concentration-specific manner indicative of diminishing cell survival and metabolism concurrent with the activation of proapoptotic proteins with both *TSC1/2*-dependent and independent consequences as previously reported (45). These findings suggested that PDGF pathway inhibition is cytocidal to renal AML cells by either stimulating proapoptotic pathways and/or interfering with glucose metabolism by tumor cells. Our results show that imatinib stimulated both early- and late-stage apoptosis in renal AML cells.

We also observed that suppressing PDGFRβ activation using the TKIs imatinib and nilotinib in renal AML cells increased gene expression of mTORC1 components mTOR and Deptor, a negative regulator of mTORC1. In addition, mTORC1-induced activation of P-S6K and P-S6-ribosomal was not affected by the TKIs. Investigators have previously evaluated the effect of mTOR pathway activation on PDGF signaling (14) but did not examine the PDGF pathway independent of mTOR in tumor growth. Arbiser and colleagues assessed the effects of TKIs in immortalized human AML cells and $Tsc2^{+/-}$ mouse cutaneous sarcoma cells but only after PDGF ligand sensitization of tumor cells (12). As such, our studies build on this prior work and pioneer comprehensive elucidation of the therapeutic mechanisms of PDGF pathway inhibition and its effect on TSC tumors. Our results suggest that TKIs act by interfering with PDGFRβ-based activation of AKT allowing for downstream mTORC1 signaling.

The comparative RNA-sequencing results implicate the inactivation of GPVI signaling as a potential contributor to the cytocidal effects of imatinib. GPVI signaling is typically activated in platelets at sites of vascular injury in response to exposed subendothelial collagens and other extracellular matrix proteins, which leads to activation of integrin receptors on platelet surfaces (46). This membrane receptor activation also triggers intracellular tyrosine phosphorylation cascades that ultimately result in the elevation of cytosolic calcium to induce platelet aggregation, hemostasis and thrombosis, and promote tumor metastasis and platelet-tumor cell interactions (47). Our results reveal that imatinib deregulates such receptor-mediated intracellular signaling leading to tumor cell death and was supported by the demonstrated increase in integrin subunit beta 3 (*ITGB3*) expression in renal AML and pulmonary LAM tumor cells and the reversal of drug effects by CGT inhibition. These bioinformatic studies have uncovered this novel cytocidal pathway induced by receptor TKIs.

Figure 3.

Differential GPVI pathway activation and endoplasmic reticulum IP_3 receptor subtype switching underlies cytocidal mechanisms of imatinib in renal AML and pulmonary LAM tumor cells. Expression states of genes in the GPVI signaling pathway in renal AML cells exposed to 10 μmol/L imatinib mesylate (**A**) versus 0.05 μmol/L Rapamycin (**C**) were contrasted to identify differential molecular signaling. Analogous comparisons were made for pulmonary LAM tumor cells treated with 10 μmol/L imatinib mesylate (**B**) versus 0.05 μmol/L Rapamycin (**D**). Gradations of red and green from low to high intensity respectively denote increasing degrees of up- and downregulation of gene expression states. Common to both cell types is the differential activation of inositol ITPR on the endoplasmic reticulum in imatinib-induced conditions compared with rapamycin-induction (in purple squares), implicating calcium fluxes as key to the cytocidal mechanisms of imatinib. Protein blots of drug-treated renal AML cells (**E**) and pulmonary LAM tumor cells (**F**) stained with antibodies against IP_3R subtypes (I, II, and III). IP_3-induced calcium efflux from the endoplasmic reticulum was inhibited using 10 μmol/L 2-aminoethyl diphenylborinate (2-APB) in renal AML cells (*, $0.05 > P < 0.003$; ϕ, $0.02 > P < 1.0E{-}06$; **G**) and pulmonary LAM tumor cells (*, $0.005 > P < 1.17E{-}07$; ϕ $P < 1.0E{-}06$; **H**) prior to induction with imatinib. 2-APB inhibition studies were performed twice per cell type in quadruplicate wells per drug concentration. Vehicle = 0.01% DMSO in respective media. Statistical comparisons were performed using multiple t tests.

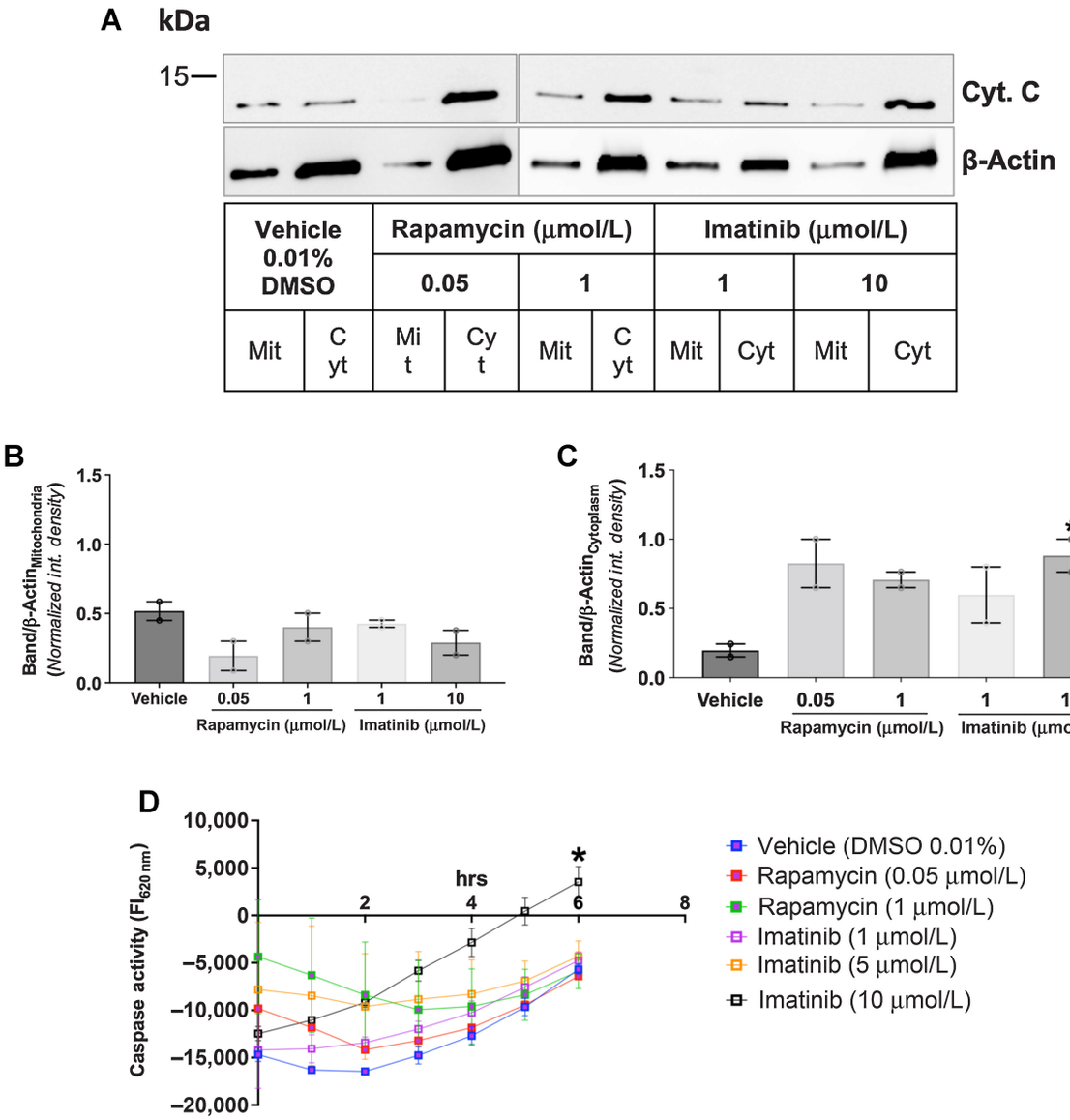

Figure 4.

Imatinib is cytocidal to UMB1949 renal AML cells by stimulating apoptosis in a concentration-dependent manner. Mitochondrial (Mit) and Cytosolic (Cyt) factions obtained from drug-induced renal AML cells (**A**) were blotted on nitrocellulose membranes and stained with anti-cytochrome C (Cyt. C) antibody. Protein blotting experiments were replicated for renal AML ($N = 2$) on different days. Semiquantitative analysis of stained Western blots of drug-induced renal AML cell mitochondrial fractions (**B**) and cytosolic fractions (**C**) using a one-way ANOVA (*, $P < 0.05$) is displayed. Caspase 3/7 activity was monitored for 6 hours following drug treatment of renal AML cells (**D**), yielding simple linear regression curves with slopes significantly different from zero only in cells exposed to 10 μmol/L imatinib by 6 hours ($y = 2760x - 13625$; $R^2 = 0.95$; *, $P < 0.0001$). Caspase activity assay was performed in duplicates/cell type.

Further exploration of the GPVI pathway identified isoform switching of inositol IP_3 receptors in the ER of tumor cells treated with higher imatinib concentrations. Preferential IP_3R isoform III expression has previously been associated with proapoptotic induction of calcium signals in the mitochondria of certain cell types, permeability transition pore formation, and the associated cytochrome C release from the mitochondria (48). The proximity of this ER IP_3R isoform III to the mitochondria in CHO cells compared with isoforms I and II has been suggested as the mechanism for its preferential effect on mitochondrial Ca^{2+} homeostasis (48). Such mitochondrial permeability events cause cell death (49) and could mechanistically underlie the tumoricidal effectiveness observed with imatinib at higher doses in renal AML and pulmonary LAM tumor cells. The imatinib-induced ER calcium efflux stimulated this known mechanism leading to cytochrome C efflux from the mitochondria to the cytosol further propagating the apoptotic process. In our investigations, blocking IP_3-induced calcium efflux using 2-APB permitted the return of renal AML and pulmonary LAM tumor cell viability to levels prior to treatment with imatinib. In addition, the role of imatinib in

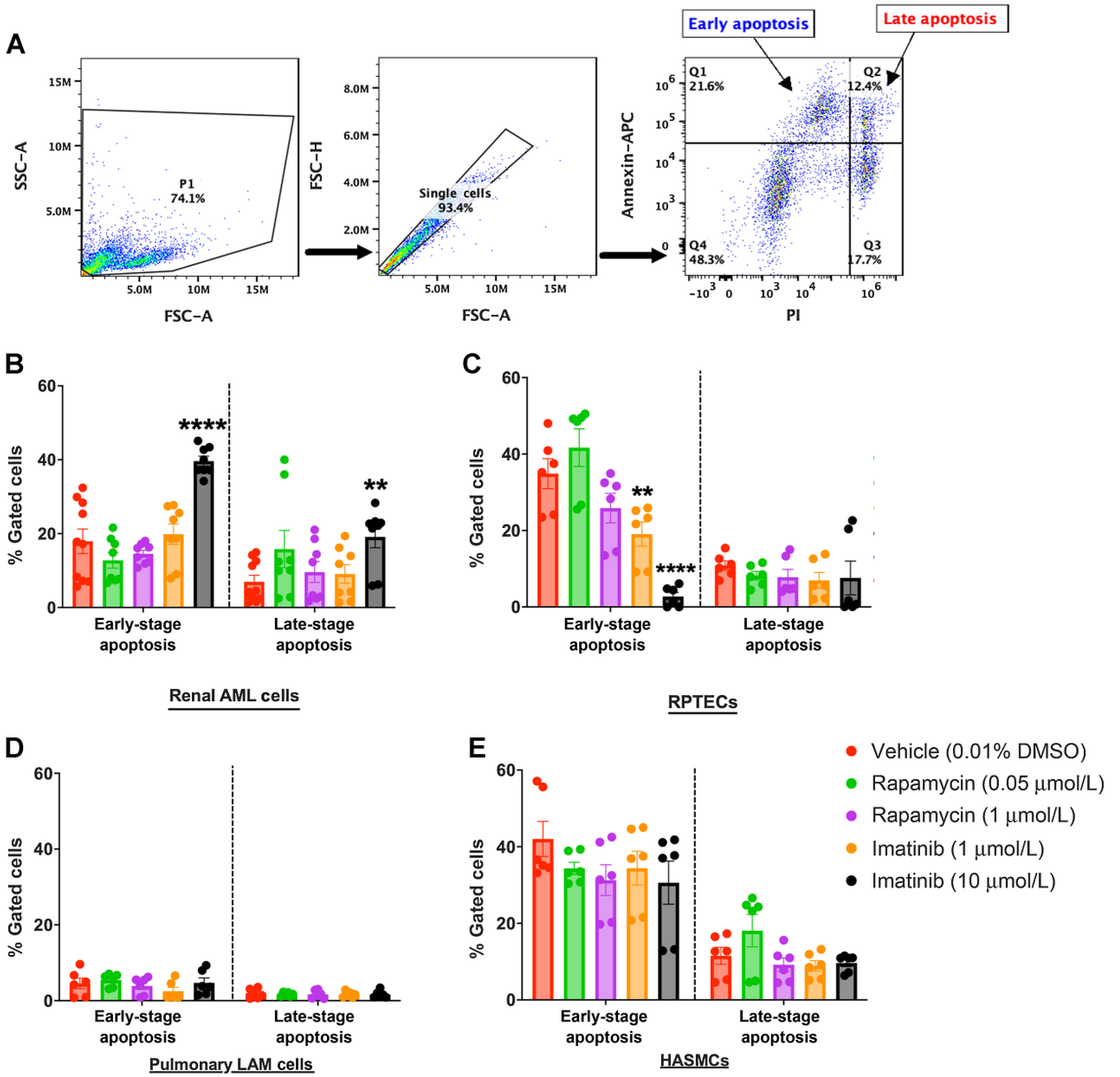

Figure 5.

Analysis of drug-induced apoptosis in renal AML and pulmonary LAM tumor cells versus control cells by flow cytometry. **A,** Drug-treated cells gated through the FSC-A versus SSC-A plot were further sorted by the ratios of height to area in forward scatter and interrogated for their ability to bind annexin only (early apoptosis) conjugated to the APC fluorophore, or both annexin and viability dye propidium iodide [PI; or sytox green (SG); late apoptosis] on a Novocyte Quanteon cell analyzer (Agilent Technologies). Unstained and single-stained cells were used as compensation controls for each experiment. **B,** Imatinib (10 µmol/L) significantly induced both early- and late-stage apoptosis in renal AML cells compared with other drug type and concentrations. Neither rapamycin nor imatinib-induced apoptosis in RPTECs; **C**), pulmonary LAM tumor cells (**D**), and HASMCs (**E**). Experiments were performed three to four different times in duplicates per experiment (ns, nonsignificant; ****, $P < 0.0001$; ***, $P = 0.0001$; **, $P < 0.005$; *, $P < 0.05$). Statistical analysis was performed using a two-way ANOVA with stage of apoptosis and drug condition as interacting factors and *post hoc* multiple comparisons for each apoptotic stage using Dunnett tests for statistical significance against control/vehicle conditions was performed. (Descriptive statistics are detailed in Supplementary Table S2.)

inducing apoptosis in TSC tumors was further confirmed *in vivo* using the *Tsc2*$^{+/-}$ mouse model demonstrating reduction of tumor area and volume in 7-month-old mice treated with imatinib compared with PBS treatment concomitant with a selective increase in the expression of Bcl2 family markers of apoptosis activation only in imatinib-treated renal tumors. Importantly, imatinib decreased tumor volume but did not prevent the emergence of new tumors suggesting that the TKI could preferentially affect tumor cells negatively only after EMT during tumor cell transformations (29).

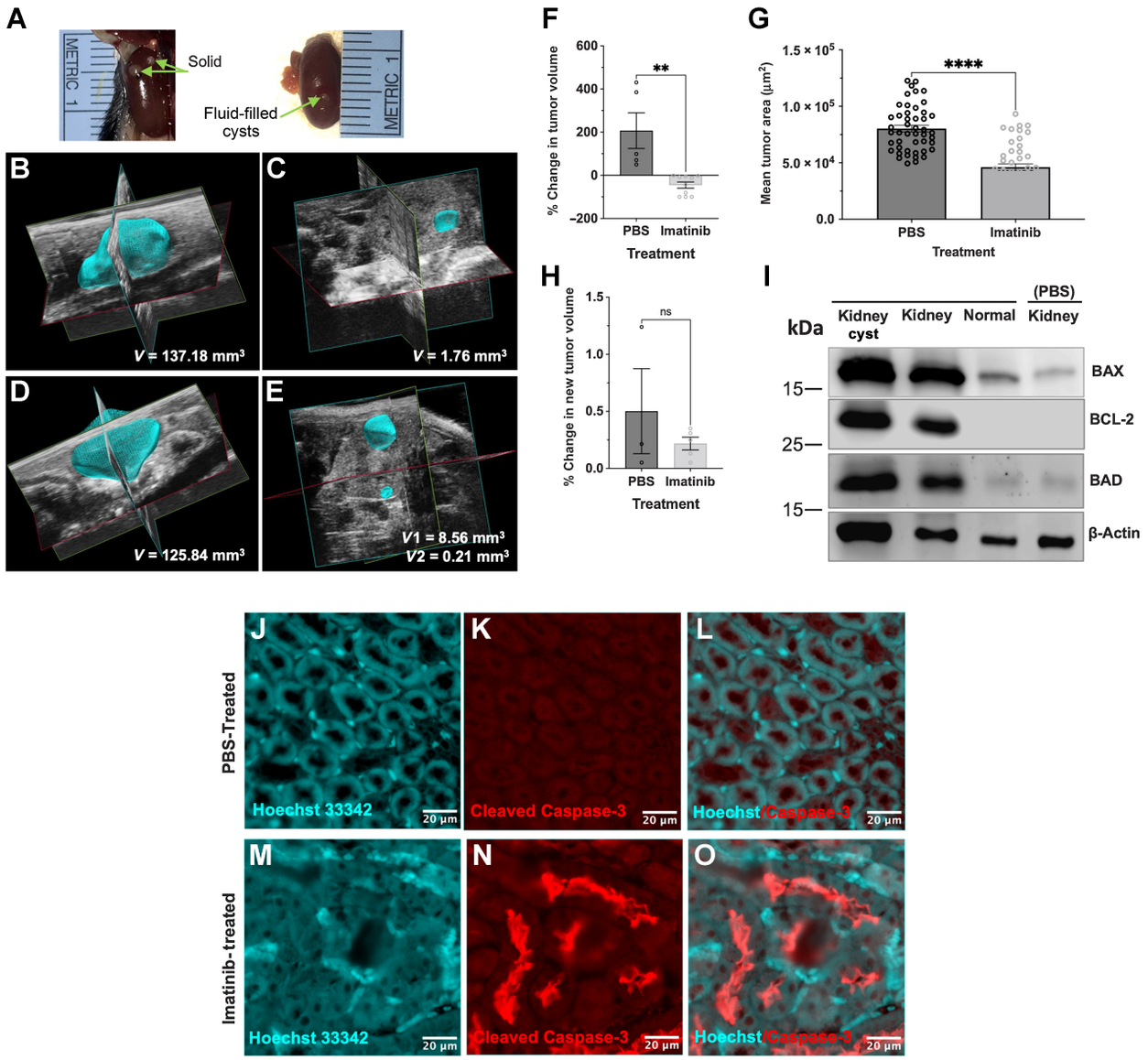

Figure 6.

Preclinical pilot study of the effect of imatinib on *Tsc2*$^{+/-}$ mice renal tumorigenesis. Representative images of renal solid tumors (**A**) and fluid-filled cysts observed in 7-month-old *Tsc2*$^{+/-}$ mice. Select 3D ultrasound scans of a large renal fluid-filled cyst in the Tsc2$^{+/-}$ mice at day 0 (**B**) and at day 30 (**D**) following daily administration of the TKI imatinib (OG, 400 mg/kg, $N = 6$ mice). Comparative images of renal tumors in the control PBS mice group (OG, 200 µL, $N = 6$ mice) are displayed at the start (**C**) and end of the experiment (**E**). Tumor volumes are displayed in each image panel, and new tumor growth can be observed as V2 in **E**. **F,** Imatinib administration resulted in a statistically significant decrease (**, $P = 0.001$) in renal tumor volume ($N = 10$ tumors) by an average of 45% compared with the PBS mice group in which tumors ($N = 5$ tumors) collectively increased in volume by an average of 207% (Supplementary Table S3). **G,** Renal cystadenomas excised from PBS-treated ($N = 3$ mice) versus imatinib-treated ($N = 3$ mice) mice after the drug study were processed into histologic hematoxylin and eosin–stained FFPE slides, and neoplastic tumor area assessed. Six tumors/mice, one slide/tumor, and two serial sections/slide at 100-µm intervals were prepared for analysis. Equal cross-sectional area of seven to eight regions of dysmorphic tissues/section for six tumor sections/drug treatment type were determined using Image J. Comparative analysis results using an unpaired *t* test indicate that mean renal tumor area in histologic sections of imatinib-treated mice ($4.61 \times 10^4 \pm 2904$ µm^2) was significantly less than mean neoplastic area in histologic renal tumor sections obtained from PBS-treated mice ($8.03 \times 10^4 \pm 2956$ µm^2) calculated using an unpaired *T* test ($N = 47$ tumor areas/drug treatment; ****, $P < 0.0001$). Mice treatment group assignment and tumor area assessment were performed blindly with regards to drug treatment status. **H,** Changes in new tumor volumes between the PBS mice and imatinib mice study groups are also graphically displayed (unpaired test: $P = 0.35$). **I,** Protein blots of renal tumors and adjacent nontumorigenic renal tissues obtained from the imatinib mice group compared with renal tumors obtained from the PBS mice group. Formalin-fixed paraffin-embedded sections (4 µmol/L) of renal cystadenomas obtained from PBS-treated *Tsc2*$^{+/-}$ mice and stained with Hoechst 33342 (**J**), anti-cleaved caspase-3 antibody conjugated to Alexa Fluor 546 (**K**) and merged Hoechst-anti-cleaved caspase images (**L**). Analogous renal tumor sections obtained from imatinib-treated mice reveal differential staining for cleaved caspase-3 (**M–O**).

The demonstrated cytocidal mechanism of the TKIs potentiates a therapy that will not only slow the growth of TSC tumors but allow for tumor elimination via GPVI signaling. The *in vitro* studies document the effectiveness of the TKI imatinib, an mTOR independent agent, in limiting pulmonary LAM and renal AML cell growth and in attenuating tumor growth in the $Tsc2^{+/-}$ mice. Therefore, these TKIs could provide additional or alternative therapies in these diseases particularly with respect to rapamycin-resistant TSC tumors (4). These results pioneer insights into an effective tumoricidal mechanism of apoptosis for TSC and LAM by inhibiting mesenchymal receptor tyrosine kinase activity with important clinical potential. The safety profile of TKIs and their extensive use in various human cancers make them an appealing potential therapeutic that can be repurposed for LAM and TSC. Future clinical trials will document the efficacy of the TKIs in TSC and LAM.

Authors' Disclosures

U. Unachukwu reports grants from Congressionally Directed Medical Research Program during the conduct of the study. J.M. D'Armiento reports grants from Congressionally Directed Medical Research Program and the National Institutes of Health. No disclosures were reported by the other authors.

Authors' Contributions

U. Unachukwu: Conceptualization, formal analysis, funding acquisition, investigation, methodology, writing–original draft, writing–review and editing. **J. Sonett:** Formal analysis, investigation, methodology, writing–review and editing. **D. Woode:** Formal analysis, investigation, methodology, writing–review and editing. **T. Shiomi:** Conceptualization, formal analysis, investigation, writing–review and editing. **K. Chada:** Supervision, writing–original draft, writing–review and editing. **J.M. D'Armiento:** Conceptualization, supervision, funding acquisition, writing–review and editing.

Acknowledgments

We thank Tina Zelonina for her work in mouse breeding and genotyping and tumor excision, Kristina Cassanova for her assistance in cell culture–based assays, and Xinran Ma for her work on cleaved caspase-3 IHC. We also thank Christopher Damoci for his technical expertise during small animal ultrasound and volume data acquisition. We thank Dr. Monica Goldklang for assistance in the collection of human tissue. This study was supported by grants from the Center for LAM and Rare Lung Diseases at Columbia University. J.M. D'Armiento was supported by NIH RO1-HL086936. U. Unachukwu and J.M. D'Armiento were supported by Congressionally Directed Medical Research Programs (CDMRP) grant (No. TS170057). Imatinib mesylate and nilotinib were supplied by Novartis International AG, Basel, Switzerland.

The publication costs of this article were defrayed in part by the payment of publication fees. Therefore, and solely to indicate this fact, this article is hereby marked "advertisement" in accordance with 18 USC section 1734.

Note

Supplementary data for this article are available at Molecular Cancer Therapeutics Online (http://mct.aacrjournals.org/).

Received March 29, 2022; revised September 26, 2022; accepted April 19, 2023; published first May 1, 2023.

References

1. Strizheva GD, Carsillo T, Kruger WD, Sullivan EJ, Ryu JH, Henske EP. The spectrum of mutations in TSC1 and TSC2 in women with tuberous sclerosis and lymphangiomyomatosis. Am J Respir Crit Care Med 2001;163:253–8.
2. Henske EP, Jozwiak S, Kingswood JC, Sampson JR, Thiele EA. Tuberous sclerosis complex. Nat Rev Dis Primers 2016;2:16035.
3. Johnson SR, Clelland CA, Ronan J, Tattersfield AE, Knox AJ. The TSC-2 product tuberin is expressed in lymphangioleiomyomatosis and angiomyolipoma. Histopathology 2002;40:458–63.
4. Valianou M, Filippidou N, Johnson DL, Vogel P, Zhang EY, Liu X, et al. Rapalog resistance is associated with mesenchymal-type changes in Tsc2-null cells. Sci Rep 2019;9:3015.
5. Kenerson H, Dundon TA, Yeung RS. Effects of rapamycin in the Eker rat model of tuberous sclerosis complex. Pediatr Res 2005;57:67–75.
6. Alves MM, Fuhler GM, Queiroz KCS, Scholma J, Goorden S, Anink J, et al. PAK2 is an effector of TSC1/2 signaling independent of mTOR and a potential therapeutic target for tuberous sclerosis complex. Sci Rep 2015;5:14534.
7. Li C, Zhang E, Sun Y, Lee PS, Zhan Y, Guo Y, et al. Rapamycin-insensitive up-regulation of adipocyte phospholipase A2 in tuberous sclerosis and lymphangioleiomyomatosis. PLoS One 2014;9:e104809.
8. Henske EP, McCormack FX. Lymphangioleiomyomatosis: a wolf in sheep's clothing. J Clin Invest 2012;122:3807–16.
9. Rosser T, Panigrahy A, McClintock W. The diverse clinical manifestations of tuberous sclerosis complex: a review. Semin Pediatr Neurol 2006;13:27–36.
10. Taveira-DaSilva AM, Moss J. Clinical features, epidemiology, and therapy of lymphangioleiomyomatosis. Clinical epidemiology 2015;7:249–57.
11. McCormack FX, Inoue Y, Moss J, Singer LG, Strange C, Nakata K, et al. Efficacy and safety of sirolimus in lymphangioleiomyomatosis. N Engl J Med 2011;364:1595–606.
12. Arbiser JL, Govindarajan B, Bai X, Onda H, Kazlauskas A, Lim SD, et al. Functional tyrosine kinase inhibitor profiling: a generally applicable method points to a novel role of platelet-derived growth factor receptor-beta in tuberous sclerosis. Am J Pathol 2002;161:781–6.
13. Farooqi AA, Siddik ZH. Platelet-derived growth factor (PDGF) signalling in cancer: rapidly emerging signalling landscape. Cell Biochem Funct 2015;33:257–65.
14. Zhang H, Bajraszewski N, Wu E, Wang H, Moseman AP, Dabora SL, et al. PDGFRs are critical for PI3K/Akt activation and negatively regulated by mTOR. J Clin Invest 2007;117:730–8.
15. Zhang H, Cicchetti G, Onda H, Koon HB, Asrican K, Bajraszewski N, et al. Loss of Tsc1/Tsc2 activates mTOR and disrupts PI3K-Akt signaling through downregulation of PDGFR. J Clin Invest 2003;112:1223–33.
16. Govindarajan B, Willoughby L, Band H, Curatolo AS, Veledar E, Chen S, et al. Cooperative benefit for the combination of rapamycin and imatinib in tuberous sclerosis complex neoplasia. Vasc Cell 2012;4:11.
17. Sawyers CL, Hochhaus A, Feldman E, Goldman JM, Miller CB, Ottmann OG, et al. Imatinib induces hematologic and cytogenetic responses in patients with chronic myelogenous leukemia in myeloid blast crisis: results of a phase II study. Blood 2002;99:3530–9.
18. Demetri GD, von Mehren M, Blanke CD, Van den Abbeele AD, Eisenberg B, Roberts PJ, et al. Efficacy and safety of imatinib mesylate in advanced gastrointestinal stromal tumors. N Engl J Med 2002;347:472–80.
19. Vittal R, Zhang H, Han MK, Moore BB, Horowitz JC, Thannickal VJ. Effects of the protein kinase inhibitor, imatinib mesylate, on epithelial/mesenchymal phenotypes: implications for treatment of fibrotic diseases. J Pharmacol Exp Ther 2007;321:35–44.
20. Giles FJ, le Coutre PD, Pinilla-Ibarz J, Larson RA, Gattermann N, Ottmann OG, et al. Nilotinib in imatinib-resistant or imatinib-intolerant patients with chronic myeloid leukemia in chronic phase: 48-month follow-up results of a phase II study. Leukemia 2013;27:107–12.
21. Lim SD, Stallcup W, Lefkove B, Govindarajan B, Au KS, Northrup H, et al. Expression of the neural stem cell markers NG2 and L1 in human angiomyolipoma: are angiomyolipomas neoplasms of stem cells? Mol Med 2007;13:160–5.
22. Townsend EA, Thompson MA, Pabelick CM, Prakash YS. Rapid effects of estrogen on intracellular Ca2+ regulation in human airway smooth muscle. Am J Physiol Lung Cell Mol Physiol 2010;298:L521–L30.
23. World Medical A. World medical association declaration of helsinki: ethical principles for medical research involving human subjects. JAMA 2013;310:2191–4.
24. Quatromoni JG, Singhal S, Bhojnagarwala P, Hancock WW, Albelda SM, Eruslanov E. An optimized disaggregation method for human lung tumors that

preserves the phenotype and function of the immune cells. J Leukoc Biol 2015;97:201–9.
25. Cheng NC, van Zandwijk N, Reid G. Cilengitide inhibits attachment and invasion of malignant pleural mesothelioma cells through antagonism of integrins alphavbeta3 and alphavbeta5. PLoS One 2014;9:e90374.
26. Peppiatt CM, Collins TJ, Mackenzie L, Conway SJ, Holmes AB, Bootman MD, et al. 2-Aminoethoxydiphenyl borate (2-APB) antagonises inositol 1,4,5-trisphosphate-induced calcium release, inhibits calcium pumps and has a use-dependent and slowly reversible action on store-operated calcium entry channels. Cell Calcium 2003;34:97–108.
27. D'Armiento J, Shiomi T, Marks S, Geraghty P, Sankarasharma D, Chada K. Mesenchymal tumorigenesis driven by TSC2 haploinsufficiency requires HMGA2 and is independent of mTOR pathway activation. Cancer Res 2016;76:844–54.
28. Unachukwu U, Trischler J, Goldklang M, Xiao R, D'Armiento J. Maternal smoke exposure decreases mesenchymal proliferation and modulates Rho-GTPase-dependent actin cytoskeletal signaling in fetal lungs. FASEB J 2017;31:2340–51.
29. Unachukwu U, Shiomi T, Goldklang M, Chada K, D'Armiento J. Renal neoplasms in tuberous sclerosis mice are neurocristopathies. iScience 2021;24:102684.
30. Festing MF. On determining sample size in experiments involving laboratory animals. Lab Anim 2018;52:341–50.
31. Jechlinger M, Sommer A, Moriggl R, Seither P, Kraut N, Capodiecci P, et al. Autocrine PDGFR signaling promotes mammary cancer metastasis. J Clin Invest 2006;116:1561–70.
32. Xu K, Liu P, Wei W. mTOR signaling in tumorigenesis. Biochim Biophys Acta 2014;1846:638–54.
33. Parkhitko A, Myachina F, Morrison TA, Hindi KM, Auricchio N, Karbowniczek M, et al. Tumorigenesis in tuberous sclerosis complex is autophagy and p62/sequestosome 1 (SQSTM1)-dependent. Proc Natl Acad Sci U S A 2011;108:12455–60.
34. Fernandes S, Iyer S, Kerr WG. Role of SHIP1 in cancer and mucosal inflammation. Ann NY Acad Sci 2013;1280:6–10.
35. Hoffman B, Liebermann DA. Apoptotic signaling by c-MYC. Oncogene 2008;27:6462–72.
36. Geng W, Ng KT, Sun CK, Yau WL, Liu XB, Cheng Q, et al. The role of proline rich tyrosine kinase 2 (Pyk2) on cisplatin resistance in hepatocellular carcinoma. PLoS One 2011;6:e27362.
37. Nam S, Williams A, Vultur A, List A, Bhalla K, Smith D, et al. Dasatinib (BMS-354825) inhibits Stat5 signaling associated with apoptosis in chronic myelogenous leukemia cells. Mol Cancer Ther 2007;6:1400.
38. Kudo Y, Iizuka S, Yoshida M, Tsunematsu T, Kondo T, Subarnbhesaj A, et al. Matrix metalloproteinase-13 (MMP-13) directly and indirectly promotes tumor angiogenesis. J Biol Chem 2012;287:38716–28.
39. Su A, He S, Tian B, Hu W, Zhang Z. MicroRNA-221 mediates the effects of PDGF-BB on migration, proliferation, and the epithelial-mesenchymal transition in pancreatic cancer cells. PLoS One 2013;8:e71309.
40. Zhu C, Kong Z, Wang B, Cheng W, Wu A, Meng X. ITGB3/CD61: a hub modulator and target in the tumor microenvironment. Am J Transl Res 2019;11:7195–208.
41. Siroky BJ, Yin H, Babcock JT, Lu L, Hellmann AR, Dixon BP, et al. Human TSC-associated renal angiomyolipoma cells are hypersensitive to ER stress. Am J Physiol Renal Physiol 2012;303:F831–44.
42. Vermes I, Haanen C, Steffens-Nakken H, Reutelingsperger C. A novel assay for apoptosis. Flow cytometric detection of phosphatidylserine expression on early apoptotic cells using fluorescein labelled Annexin V. J Immunol Methods 1995;184:39–51.
43. Yang J, Kalogerou M, Gallacher J, Sampson JR, Shen MH. Renal tumours in a Tsc1+/– mouse model show epigenetic suppression of organic cation transporters Slc22a1, Slc22a2 and Slc22a3, and do not respond to metformin. Eur J Cancer 2013;49:1479–90.
44. Kaur J, Debnath J. Autophagy at the crossroads of catabolism and anabolism. Nat Rev Mol Cell Biol 2015;16:461–72.
45. Laplante M, Sabatini DM. mTOR signaling at a glance. J Cell Sci 2009;122:3589–94.
46. Gupta S, Cherpokova D, Spindler M, Morowski M, Bender M, Nieswandt B. GPVI signaling is compromised in newly formed platelets after acute thrombocytopenia in mice. Blood 2018;131:1106–10.
47. Mammadova-Bach E, Gil-Pulido J, Sarukhanyan E, Burkard P, Shityakov S, Schonhart C, et al. Platelet glycoprotein VI promotes metastasis through interaction with cancer cell–derived galectin-3. Blood 2020;135:1146–60.
48. Mendes CC, Gomes DA, Thompson M, Souto NC, Goes TS, Goes AM, et al. The type III inositol 1,4,5-trisphosphate receptor preferentially transmits apoptotic Ca2+ signals into mitochondria. J Biol Chem 2005;280:40892–900.
49. Shen L, Wen N, Xia M, Zhang Y, Liu W, Xu Y, et al. Calcium efflux from the endoplasmic reticulum regulates cisplatin-induced apoptosis in human cervical cancer HeLa cells. Oncol Lett 2016;11:2411–9.